Multi-frequency recirculating planar magnetrons

Geoffrey B. Greening, Nicholas M. Jordan, Steven C. Exelby, David H. Simon, Y. Y. Lau, and Ronald M. Gilgenbach
Plasma, Pulsed Power, and Microwave Laboratory, Department of Nuclear Engineering and Radiological Sciences, University of Michigan, Ann Arbor, Michigan 48109, USA

(Received 14 July 2016; accepted 25 July 2016; published online 18 August 2016)

The multi-frequency recirculating planar magnetron (MFRPM) is the first magnetron capable of simultaneous generation of significantly different output frequencies (1 and 2 GHz) in a single operating pulse. Design and simulation of a prototype MFRPM were followed by hardware fabrication and experimental verification using the Michigan Electron Long Beam Accelerator with a Ceramic insulator at −300 kV, 1–5 kA, and 0.14–0.23 T axial magnetic field. Preliminary results demonstrated simultaneous generation of microwave pulses near 1 GHz and 2 GHz at powers up to 44 MW and 21 MW, respectively, with peak total efficiencies up to 9%. *Published by AIP Publishing.*
[http://dx.doi.org/10.1063/1.4961070]

High-power microwaves (HPM) have a number of applications in the fields of industry, fusion science, and defense,[1–3] with the latter including counter-electronics. The cavity magnetron is generally accepted as the standard for compactness and high microwave power,[4] though it has some limits in counter-electronics applications due to being a narrow-band device. Considerable research has therefore been devoted to improving the range of accessible frequencies that can be produced using a single magnetron.

One method of producing different frequencies involves operating the magnetron in different resonant electromagnetic modes by adjusting the operating voltage and axial magnetic field.[5] This approach requires flexibility in the range of voltages and/or magnetic fields that can be applied to the magnetron. The method is also predicated on a slow-wave structure (SWS) having (1) very different frequencies with (2) similar phase velocities that are all (3) well-matched to the microwave extractor. The second condition is particularly difficult to achieve in magnetron design and is typically infeasible at relativistic voltages due to the incorporation of features prone to arcing, such as anode straps. Operating the magnetron at very different frequencies (and therefore very different phase velocities) demands that the electron $\vec{E} \times \vec{B}$ drift velocity be very different for the two modes, which usually compromises efficiency (due to having a fast phase velocity) or output power (due to having an excessively slow phase velocity). Mode-hopping in relativistic devices is possible due to cathode plasma expansion,[6] though this is generally undesirable due to the lack of temporal control, and does not produce simultaneous emission at the two frequencies. In addition, as stated previously, the neighboring modes (between which hopping has been observed) tend to be relatively close in frequency and phase velocity, though this depends on the dispersion relation of a given SWS.

Another approach used to produce different frequencies involves the use of mechanical plungers to modify the resonant frequency of a given mode.[7] While this method is effective, it is complex due to the mechanical-vacuum interface, ultimately limited in the range of available tunability (e.g., the aforementioned reference quotes 33% tunability), and cannot produce different frequencies simultaneously.

The last approach involves the incorporation of two different SWSs in a single HPM source. Such a concept has been presented in the literature for other devices, but a dual-frequency magnetron has not yet been investigated. Some examples of dual-frequency concepts include magnetically insulated line oscillators,[8,9] klystron-like concepts,[10] and backward-wave oscillators.[11]

In this letter, the dual SWS approach is employed using the Recirculating Planar Magnetron (RPM)[12] geometry to design, fabricate, and experimentally demonstrate a prototype multi-frequency RPM (MFRPM). Fig. 1 shows the MFRPM prototype and experimental configuration. The RPM has several potential advantages over conventional cylindrical cavity magnetrons and has considerable flexibility in its design, both of which have been addressed in the literature.[13–17] The design approach is discussed in detail, followed by some preliminary experimental data validating the MFRPM concept.

The MFRPM prototype is designed around one of the existing 1 GHz planar cavity arrays that formed the SWSs in the RPM-12A anode used in previous RPM experiments.[14,16] That SWS, hereafter referred to as the L-band oscillator (LBO), is comprised of 6 resonant cavities having cavity depth $h = 6.31$ cm, cavity width $w = 1.92$ cm, and circuit pitch (or, equivalently, the width of a vane plus the width of a cavity) $L = 3.84$ cm, with a vane width equal to the cavity width. The π-mode (a phase advance of 180° per vane) is designed to operate at 1 GHz with a phase velocity of $0.26c$. The axial length of the LBO anode is 11 cm, which is less than half the 15 cm free-space 1 GHz wavelength in order to impede axial mode formation.

The second SWS for the MFRPM prototype is designed for π-mode operation at 2 GHz and is hereafter referred to as the S-band oscillator (SBO). The reason for this choice of frequency was to investigate whether moderate coupling between the oscillators (e.g., by way of a Mode-Control Cathode (MCC)[15]), given identical phase velocities for the two oscillators, might lead to frequency-locked behavior,

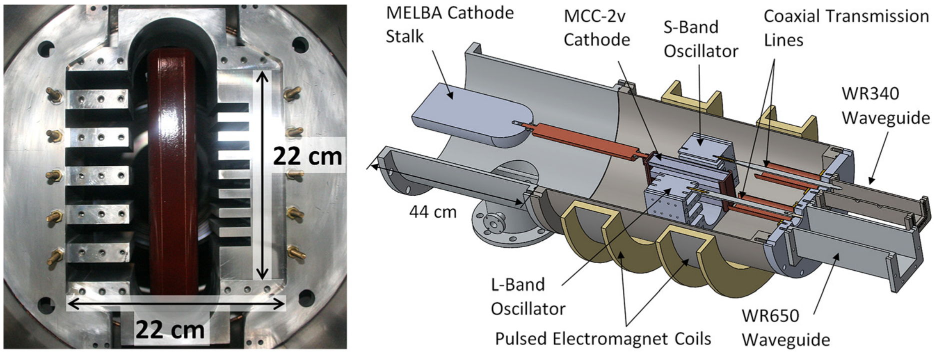

(a) (b)

FIG. 1. Experimental hardware and configuration. (a) Photograph of MFRPM prototype viewed from the front. The central structure is the cathode. The anode consists of 6-cavity 1 GHz and 8-cavity 2 GHz planar cavity arrays. (b) Cross-sectional view of the experimental configuration.

wherein $f_2 = 2 \times f_1$, in a way that is analogous to peer-to-peer magnetron phase-locking.[18,19] The SBO was designed using the two equations below with parameter constraints based on experimental hardware limitations

$$\frac{\cot(\omega h/c)}{(\omega h/c)} = \left(\frac{w}{L}\right) \sum_{n=-\infty}^{\infty} \mathrm{sinc}^2\left(\frac{\beta_n w}{2}\right) \frac{\coth \gamma_n b}{\gamma_n h}, \quad (1)$$

$$V_{\mathrm{BH}} = bB\beta_p c - \left(1 - \sqrt{1-\beta_p^2}\right)\frac{mc^2}{e}. \quad (2)$$

Eq. (1) is based on the existing theory for infinite, two-dimensional, planar cavity arrays.[20,21] In Eq. (1), h is the cavity depth, w is the cavity width, L is the circuit pitch, b is the anode-cathode (AK) gap spacing, ω is the angular frequency, c is the speed of light, $\beta_n = \beta_0 + 2n\pi/L$ and $\gamma_n = \sqrt{\beta_n^2 - (\omega/c)^2}$ for $n = 0, \pm1, \pm2, \ldots$, and β_0 is the propagation constant ($\beta_0 = 2\pi/\lambda_g$ for a guide wavelength λ_g).

Eq. (2) is the well-known Buneman-Hartree condition for magnetron beam-wave synchronism,[22–24] which is a relativistic, single-particle treatment that relates the operating DC voltage, magnetic field, and AK gap spacing to achieve electron drift velocity synchronism (at the anode) with RF waves propagating at a given phase velocity on the slow-wave structure. In Eq. (2), V_{BH} is the operating voltage for synchronism, b is the AK gap spacing, B is the magnetic field, and β_p is the c-normalized RF phase velocity ($\beta_p = v_p/c = \omega/\beta_0 c$).

By using Eqs. (1) and (2), preliminary dimensions of the SBO could be determined subject to several constraints. As mentioned earlier, the desired operating mode for the SBO is the π-mode, which is the same as the LBO. The DC voltage for operation in the π-mode (V_{BH}) is fixed at the Michigan electron long beam accelerator with ceramic insulator (MELBA-C) operating voltage (-300 kV). The maximum magnetic field B in the AK gap is limited by the pulsed electromagnet specifications and both the choice and amount of anode material,[17] but generally, the minimum necessary magnetic field for synchronism should not exceed 0.2 T. The cathodes used for the RPM have large surface areas and operate in an explosive emission, space-charge-limited regime, which makes it particularly difficult to achieve uniform electron emission.[25] This may be exacerbated if the AK gap spacing is appreciably different for the SBO relative to the LBO, so each planar cavity array in the MFRPM has the same AK gap spacing b. Given the identical b (and therefore identical beam velocity), the SBO must have the same RF phase velocity β_p as the LBO. Since the frequency of interest for the SBO was chosen to be 2 GHz (an integer multiple of the LBO), ω is also constrained. For simplicity, the vane width and cavity width were the same in all candidate designs.

Further refinement of the cavity array dimensions used the 3D particle-in-cell code MAGIC[26] to estimate the degree of beam loading on the frequency and adjust the planar cavity array dimensions to compensate. The final SBO design is composed of 8 resonant cavities having cavity depth $h = 3.18$ cm, cavity width $w = 0.96$ cm, and circuit pitch $L = 1.92$ cm. The axial length of the SBO anode is the same as the LBO, which could potentially support axial mode formation, but is necessary in order to use the existing LBO and cylindrical recirculation bends from the RPM-12A. The simple planar cavity array design suffers decreasing mode separation as the cavity number increases, so an 8 cavity design was chosen over a larger 12 cavity design to reduce the likelihood of mode competition.

Microwave power extraction is accomplished using the same approach used for the RPM-12A.[16] The centermost vane of each oscillator is connected to an antenna, which forms the inner conductor of a coaxial transmission line axially downstream from the magnetron. The coaxial transmission line is then transitioned to WR 650 and WR 340 waveguide for the LBO and SBO, respectively, using coax-to-waveguide mode converters. The waveguide outputs include the vacuum windows, directional couplers for microwave sampling, and Eccosorb-matched RF loads. It is important to note that the axial extraction assembly is a relatively straightforward implementation that could be applied within the limits of existing hardware and is not optimized for maximum power extraction. External quality factors for the LBO and SBO at their respective cold-tube π-mode frequencies are approximately 500.

The cathode is the MCC-2v, which uses 3.61 cm^2 velvet squares as the electron emitters attached using conducting silver epoxy adhesive to both sides of each of the 5 bars forming the structure, and provides a 2.6 cm AK gap.[16] A MCC is geometrically similar to the transparent cathode[27] in that it provides a source of both electric[28] and magnetic priming,[29] but it also serves to increase the coupling between each of the SWSs.[15] Emission from non-velvet surfaces is reduced using Glyptal insulating enamel to maintain a magnetron impedance near the MELBA-C design specification of 100–150 Ω. The axial magnetic field is produced using two

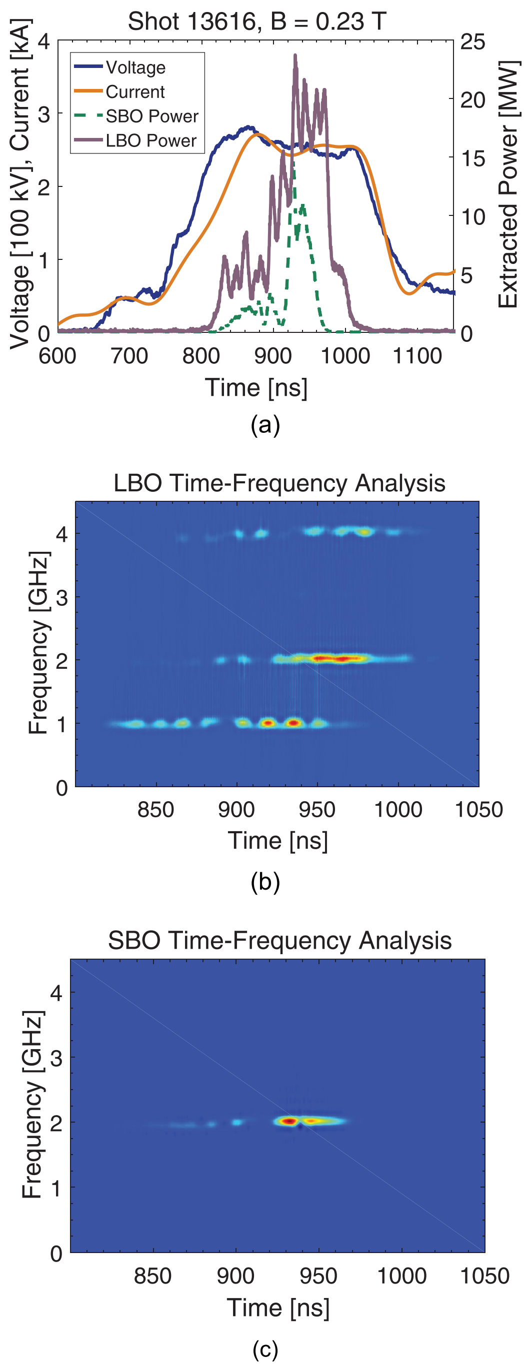

FIG. 2. Sample experimental MELBA-C shot no. 13616. (a) Shot plot illustrating voltage, current, and detected RF powers for both oscillators. Peak LBO (SBO) powers were 24 MW (15 MW) at 0.98 GHz (2.0 GHz). (b) Time-frequency analysis for the LBO. (c) Time-frequency analysis for the SBO.

electromagnet coils in a pseudo-Helmholtz configuration centered on the MFRPM anode. The time delay between triggering the electromagnets and MELBA-C is chosen to allow diffusion of the magnetic field into the structure with a peak occurring in the center of each SWS. Axial magnetic fields ranged from 0.14 to 0.23 T. Operating pressures are 10^{-7}–10^{-6} Torr. The microwave signal sampled from each directional coupler is split using a 3 dB power divider, with one signal recorded directly using a fast Tektronix 7404 oscilloscope (10 Gsamples/s), and the other signal fed to calibrated Agilent 8472B low-barrier Schottky diodes for power measurement captured using a Tektronix 3054 oscilloscope. Attenuation of all components (directional couplers, cables, splitters, and attenuators) is determined at the design frequencies of the two oscillators. Operating voltage is determined using a $CuSO_4$ voltage divider, and current is determined using time-integrated Rogowski coil signals, each captured using the Tektronix oscilloscope.

Results for 123 shots were obtained. Currents and voltages at peak microwave power were 1.7–5.3 kA and 170–288 kV, respectively, with magnetron impedances from 44 to 155 Ω. Fig. 2 presents data illustrating typical behavior of the MFRPM prototype. The LBO begins oscillating first, which is consistent with expectations from the standpoint of the analytic solutions to Eq. (1). The derivation of Eq. (1) involves solutions for the fringing RF fields from the cavities whose magnitudes scale as $\sinh(\gamma_n x) \simeq \sinh(\pi x/L)$ for the π-mode in the AK gap, where x is the distance from the cathode surface; this suggests that the electric field magnitude decays with x/L. Since L is twice as large for the LBO than the SBO, the fringing L-band fields are considerably stronger and the Brillouin electron hub can reasonably be expected to excite LBO startup earlier than the SBO for equal hub height, which is the case here given the AK gap is the same. A time-frequency analysis (TFA)[30] of both the LBO and SBO signals reveals an intriguing feature, namely the 2 and 4 GHz harmonic content of the LBO signal. The LBO 2 GHz harmonic is not always the same frequency as the SBO fundamental, so the origin of the harmonic is not necessarily due to the SBO.[31] Characterizing the power content and the origin of these harmonics will be the focus of future work.

Fig. 3 shows the peak output power for both oscillators vs. magnetic field. Best operation was observed at the maximum field that could be produced by the electromagnets, with peak LBO and SBO powers as high as 44 MW and 21 MW, respectively, with peak total efficiencies (based on the peak of the sum of the power traces for both oscillators) up to 9%. Here, total efficiency is defined as the ratio of peak output power to the product of voltage and current to the cathode. The high external Q of the oscillators strongly implies that improvements in the extraction coupling and load characteristics would lead to improved powers and efficiencies.[32] Given that the solution to Eq. (2) for an operating voltage of 300 kV and a 2.6 cm AK gap is a magnetic field of 0.16 T, the high magnetic fields for best operation are

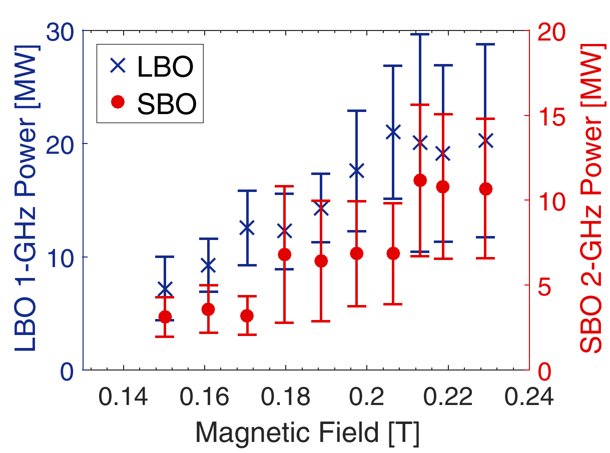

FIG. 3. Experimental powers for both oscillators vs. magnetic field.

somewhat surprising. A possible explanation may be the early formation of cathode plasma, effectively shrinking the AK gap and therefore requiring a higher magnetic field to maintain beam-wave synchronism.[6]

These results validate the concept of the multi-frequency recirculating planar magnetron prototype as a means of simultaneously generating microwaves at two different frequencies using two slow-wave structures. Using a combination of analytic theory and particle-in-cell simulations, a set of simple planar cavity arrays produced 16 ± 8 MW and 8 ± 5 MW at approximately 1 GHz and 2 GHz, respectively, over the broad range of magnetic fields tested, with peak powers of 44 MW and 21 MW at the oscillators' respective design frequencies. Future work will focus on characterizing the operation of the prototype, including the L-band oscillator harmonics.

The authors wish to acknowledge the support provided by the Office of Naval Research under Grant Nos. N00014-13-1-0566 and N00014-16-1-2353, and L-3 Communications Electron Devices.

[1] J. Benford, J. A. Swegle, and E. Schamiloglu, *High Power Microwaves*, 3rd ed. (CRC Press, New York, 2016).
[2] R. M. Gilgenbach, M. E. Read, K. E. Hackett, R. Lucey, B. Hui, V. L. Granatstein, K. R. Chu, A. C. England, C. M. Loring, O. C. Eldridge, H. C. Howe, A. G. Kulchar, E. Lazarus, M. Murakami, and J. B. Wilgen, Phys. Rev. Lett. **44**, 647 (1980).
[3] N. Friedman, *The Naval Institute Guide to World Naval Weapon Systems*, 5th ed. (Naval Institute Press, 2006).
[4] R. M. Gilgenbach, in *Modern Microwave and Millimeter-Wave Power Electronics*, edited by R. J. Barker, J. H. Booske, N. C. Luhmann, and G. S. Nusinovich, 1st ed. (Wiley-IEEE Press, Hoboken, NJ, 2005), pp. 289–342.
[5] T. A. Treado, W. O. Doggett, G. E. Thomas, R. S. Smith, J. Jackson-Ford, and D. J. Jenkins, IEEE Trans. Plasma Sci. **16**, 237 (1988).
[6] D. Price, J. S. Levine, and J. N. Benford, IEEE Trans. Plasma Sci. **26**, 348 (1998).
[7] J. S. Levine, B. D. Harteneck, and H. D. Price, Proc. SPIE **2557**, 74–79 (1995).
[8] J.-C. Ju, Y.-W. Fan, H.-H. Zhong, and T. Shu, IEEE Trans. Plasma Sci. **37**, 2041 (2009).
[9] X. Zhang, Y. Li, Z. Li, H. Zhong, and B. Qian, Rev. Sci. Instrum. **86**, 104703 (2015).
[10] J. He, Y. Cao, J. Zhang, T. Wang, and J. Ling, Laser Part. Beams **29**, 479 (2011).
[11] W. Ting, Q. Bao-liang, Z. Jian-de, Z. Xiao-ping, C. Yi-bing, and Z. Qiang, Phys. Plasmas **18**, 013107 (2011).
[12] R. M. Gilgenbach, Y. Y. Lau, D. M. French, B. W. Hoff, J. Luginsland, and M. Franzi, "Crossed field device," U.S. patent 8841867b2 (September 23, 2014).
[13] R. M. Gilgenbach, Y.-Y. Lau, D. M. French, B. W. Hoff, M. Franzi, and J. Luginsland, IEEE Trans. Plasma Sci. **39**, 980 (2011).
[14] M. A. Franzi, R. M. Gilgenbach, B. W. Hoff, D. A. Chalenski, D. Simon, Y. Y. Lau, and J. Luginsland, IEEE Trans. Plasma Sci. **41**, 639 (2013).
[15] M. Franzi, R. Gilgenbach, Y. Y. Lau, B. Hoff, G. Greening, and P. Zhang, Phys. Plasmas **20**, 033108 (2013).
[16] M. A. Franzi, G. B. Greening, N. M. Jordan, R. M. Gilgenbach, D. H. Simon, Y. Y. Lau, B. W. Hoff, and J. Luginsland, IEEE Trans. Plasma Sci. **43**, 1675 (2015).
[17] N. M. Jordan, G. B. Greening, B. W. Hoff, S. S. Maestas, S. C. Exelby, and R. M. Gilgenbach, IEEE Trans. Plasma Sci. **44**, 1258 (2016).
[18] J. Benford, H. Sze, W. Woo, R. R. Smith, and B. Harteneck, Phys. Rev. Lett. **62**, 969 (1989).
[19] E. J. Cruz, B. W. Hoff, P. Pengvanich, Y. Y. Lau, R. M. Gilgenbach, and J. W. Luginsland, Appl. Phys. Lett. **95**, 191503 (2009).
[20] J. W. Gewartowski and H. A. Watson, *Principles of Electron Tubes* (D. Van Nostrand, Princeton, NJ, 1965).
[21] Y. Y. Lau and D. Chernin, Phys. Fluids B **4**, 3473 (1992).
[22] *Microwave Magnetrons*, edited by G. B. Collins (McGraw-Hill, New York, 1948).
[23] Y. Y. Lau, in *High-Power Microwave Sources*, edited by V. L. Granatstein and I. Alexeff (Artech House, Norwood, MA, 1987), pp. 309–349.
[24] Y. Y. Lau, J. W. Luginsland, K. L. Cartwright, D. H. Simon, W. Tang, B. W. Hoff, and R. M. Gilgenbach, Phys. Plasmas **17**, 033102 (2010).
[25] D. Shiffler, M. Ruebush, M. LaCour, K. Golby, R. Umstattd, M. C. Clark, J. Luginsland, D. Zagar, and M. Sena, Appl. Phys. Lett. **79**, 2871 (2001).
[26] B. Goplen, L. Ludeking, D. Smith, and G. Warren, Comput. Phys. Commun. **87**, 54 (1995).
[27] M. Fuks and E. Schamiloglu, Phys. Rev. Lett. **95**, 205101 (2005).
[28] M. C. Jones, V. B. Neculaes, Y. Y. Lau, R. M. Gilgenbach, and W. M. White, Appl. Phys. Lett. **85**, 6332 (2004).
[29] B. W. Hoff, R. M. Gilgenbach, N. M. Jordan, Y. Y. Lau, E. J. Cruz, D. M. French, M. R. Gomez, J. C. Zier, T. A. Spencer, and D. Price, IEEE Trans. Plasma Sci. **36**, 710 (2008).
[30] C. W. Peters, W. J. Williams, R. M. Gilgenbach, Y. Y. Lau, R. L. Jaynes, W. E. Cohen, M. R. Lopez, and T. A. Spencer, *Advanced Signal Processing Algorithms, Architectures, and Implementations X* (2000), Vol. **4116**, pp. 1–8.
[31] C. F. Dong, P. Zhang, D. Chernin, Y. Y. Lau, B. W. Hoff, D. H. Simon, P. Wong, G. B. Greening, and R. M. Gilgenbach, IEEE Trans. Electron Devices **62**, 4285 (2015).
[32] A. Sayapin, Y. Hadas, and Y. E. Krasik, Appl. Phys. Lett. **95**, 074101 (2009).